JOURNAL OF GEOPHYSICAL RESEARCH, VOL. 114, D01103, doi:10.1029/2008JD009961, 2009

Seasonal variations of global lightning activity extracted from Schumann resonances using a genetic algorithm method

Heng Yang,[1,2] Victor P. Pasko,[1] and Gabriella Sátori[3]

Received 13 February 2008; revised 23 September 2008; accepted 24 October 2008; published 10 January 2009.

[1] A three-dimensional Finite Difference Time Domain (FDTD) model of the Earth-ionosphere cavity with a realistic conductivity profile is employed to study the global lightning activity using the observed intensity variations of Schumann resonances (SR). Comparison of the results derived from our FDTD model and the previous studies by other authors on related subjects shows that Schumann resonance is a good probe to indicate the seasonal variations of lightning activity in three main thunderstorm regions (Africa, southeast Asia, and South America). An inverse method based on genetic algorithms is developed to extract information on lightning intensity in these three regions from observed SR intensity data. Seasonal variations of the lightning activity in three thunderstorm centers are clearly observed in our results. Different SR frequency variations associated with seasonal variations of global lighting activity are also discussed.

Citation: Yang, H., V. P. Pasko, and G. Sátori (2009), Seasonal variations of global lightning activity extracted from Schumann resonances using a genetic algorithm method, *J. Geophys. Res.*, *114*, D01103, doi:10.1029/2008JD009961.

1. Introduction

[2] The space separating the Earth and the ionosphere forms a dissipative closed cavity (Earth-ionosphere cavity) that can support electromagnetic quasi-standing waves with wavelength comparable to the planetary dimensions. The conduction losses in the cavity lead to the effect that only electromagnetic signals below 100 Hz can propagate long distances without suffering serious attenuation. The interference between the direct wave and the antipodal wave produces global resonances [e.g., *Sentman*, 1995; *Nickolaenko and Hayakawa*, 2002, p. 158].

[3] The resonance properties of the Earth-ionosphere cavity were first predicted and discussed by *Schumann* [1952], so these resonances are commonly referred to as Schumann resonances (SR). SR are mainly excited by the cloud-to-ground lighting discharges in the atmosphere, and carry information about the global lightning activity in three main thunderstorm regions (Africa, southeast Asia, and South America) and electromagnetic properties of the lower ionosphere. The long-term SR records collected at several different stations have been reported in many papers [e.g., *Sátori et al.*, 1996; *Nickolaenko et al.*, 1998; *Price and Melnikov*, 2004; *Yatsevich et al.*, 2006; *Sekiguchi et al.*, 2008]. The clear diurnal and seasonal variations of SR power and frequency were observed. Those observations of SR have been used in many applications to remotely sense the global lightning activity, the global climate variation, and the planetary-scale variability of the lower ionosphere [e.g., *Williams*, 1992]. We note that all of above SR records are obtained in the Northern Hemisphere, and there are no long-term SR measurements in the Southern Hemisphere published in the journal papers so far.

[4] The Finite-Difference Time-Domain (FDTD) method [e.g., *Taflove and Hagness*, 2000], as first proposed by *Yee* [1966], represents one of the simplest and most flexible means to discretize the differential form of Maxwell's equations for finding electromagnetic solutions in a medium with arbitrary inhomogeneities, and several reports about applications of this technique to solution of VLF/ELF propagation problems in the Earth-ionosphere cavity have recently appeared in the literature [e.g., *Pasko et al.*, 1998; *Cummer*, 2000; *Berenger*, 2002; *Hayakawa and Otsuyama*, 2002; *Otsuyama et al.*, 2003; *Simpson and Taflove*, 2004, 2007; *Soriano et al.*, 2005; *Hu and Cummer*, 2006; *Simpson*, 2008]. Besides the FDTD technique, several other numerical and analytical techniques have been successfully applied to solve SR problems [e.g., *Morente et al.*, 2003; *Kirillov*, 2002, 2005; *Mushtak and Williams*, 2002; *Ando et al.*, 2005; *Ando and Hayakawa*, 2007; *Greifinger et al.*, 2005, 2007]. In our previous studies, a 3D FDTD model has been developed and applied to describe the variation of SR parameters with the external perturbations, such as solar proton events and X-ray bursts [*Yang and Pasko*, 2005], the diurnal and seasonal variations of SR parameters with the global lightning activity [*Yang and Pasko*, 2006], and SR problems on the other celestial bodies in the Solar System, for example, Titan, Venus, and Mars [*Yang et al.*, 2006]. Since cloud-to-ground flashes with positive polarity

[1]CSSL Laboratory, Pennsylvania State University, University Park, Pennsylvania, USA.
[2]Now at Department of Electrical and Computer Engineering, University of Houston, Houston, Texas, USA.
[3]Geodetic and Geophysical Research Institute, Hungarian Academy of Sciences, Sopron, Hungary.

0148-0227/09/2008JD009961$09.00

associated with sprites excite Schumann resonances with amplitudes several times greater than the background resonances, some recent research has used Schumann resonances as proxies for lightning source locations to indicate where sprites might be located [e.g., *Huang et al.*, 1999; *Sato and Fukunishi*, 2003].

[5] The genetic algorithm (GA) is an optimization and search technique based on the principles of genetics and natural selection. Owing to its powerful ability to optimize a large number of variables with extremely complex cost surfaces, GA has become a popular method to solve the optimization problems [*Haupt and Haupt*, 2004]. In our previous studies [*Yang and Pasko*, 2006, 2007], the time dynamics of the global lightning activity in Africa, southeast Asia and South America were taken from previously published sources [e.g., *Sentman and Fraser*, 1991]. In the present paper, these dynamics during different seasons are inversely calculated from experimental Schumann resonance power measurements [e.g., *Price and Melnikov*, 2004] using a new inverse method based on GA [*Haupt and Haupt*, 2004]. The associated connection between SR frequency variations and the global lightning activity during different seasons is also discussed.

2. Model Formulation

[6] In the present paper, a 3D spherical FDTD model [*Yang and Pasko*, 2005] is employed to solve the ELF problems in the Earth-ionosphere cavity. Determining the cell size for obtaining accurate results is the first step in the development of a FDTD model. Generally, the cell size is chosen as one tenth of the wavelength which we are interested in. This standard has been widely used in the FDTD study and commercial software development. In our model, the cell size is $9^\circ \times 9^\circ$ (1000 km $\times$ 1000 km). This resolution can provide a high precision for the waves with a wavelength more than 10000 km (or frequency <30 Hz). Since we only study on the first mode (7.5–8.0 Hz) in the present paper, this resolution is high enough to solve the problem. In r direction, the grid size is chosen to be 5 km. The time step Δt is determined by the Courant condition (see equation (1)) [e.g., *Taflove and Hagness*, 2000, p. 136].

$$\Delta t < \frac{1}{c\sqrt{\frac{1}{S_r^2}+\frac{1}{S_\theta^2}+\frac{1}{S_\phi^2}}}, \tag{1}$$

where c is the speed of light. S_r, S_θ and S_ϕ are the smallest cell size in r, θ and ϕ directions, respectively. The cavity is excited by a vertical lightning current with 5 km length, which has a linear rise time 500 μs and exponential fall with timescale 5 ms. The reported results for frequencies <40 Hz are not sensitive to the specifics of the chosen lightning current waveform.

[7] The conductivity profiles employed in this paper are derived following the method we have reported in our previous work [*Yang and Pasko*, 2006]. At altitude <60 km, the total conductivity is dominated by the ion conductivity, σ_i. The ion conductivity profile is taken from *Hale* [1984] and *Huang et al.* [1999]. Above 60 km, the electron conductivity σ_e is dominant over the ion conductivity, and can be determined by $\sigma_e = N_e q_e \mu_e$ where q_e is the charge of the electron, N_e is the electron number density derived from International Reference Ionosphere (IRI) model [*Bilitza*, 2001], μ_e is the mobility of the electrons given by $\mu_e = 1.36 N_0/N \frac{m^2}{Vs}$, where $N_0 = 2.688 \times 10^{25}$ m^{-3}, and N is altitude-dependent number density of air molecules [*Pasko et al.*, 1997]. The electron density in the cavity, N_e, is derived from the IRI model for representative days of 15 January 2000, 15 May 2000, and 15 October 2000 from 0000 UT to 2400 UT, to account for the diurnal electron density variations during winter, spring and fall seasons, respectively. The total conductivity σ is derived as $\sigma = \sigma_i + \sigma_e$. The calculated representative day and night conductivity profiles can be found in Figure 2 of *Yang and Pasko* [2006].

[8] In the Earth-ionosphere cavity, the lightning activity mainly concentrates in three major areas: southeast Asia, Africa and South America. The magnitude of the lightning activity in these three regions reaches a peak at different time in the diurnal cycle at approximately 0800, 1400, and 2200 UT, respectively [e.g., *Sentman*, 1995]. In our simulations, the peak power of the first SR mode is calculated every 1.2 hours from 0000 UT to 2400 UT. Since the Earth-ionosphere cavity can be considered as a linear system, we can deal with these three sources separately. At each time point (e.g., 00 UT, 01.12 UT), three simulations are run. Only one source with unit magnitude is located at Africa, Asia and America, respectively, in each simulation. The total signal used in the final analysis can be expressed by the sum of the three waveforms multiplied by the lightning activity magnitude in three lightning centers. The mutual delay of pulses arriving from individual lightning centers has been automatically calculated and included in those waveforms [*Yang and Pasko*, 2006]. The corresponding longitudinal positions of those three regions are derived from OTD maps of *Christian et al.* [2003]. For Africa and Asia, the centers are placed at 27°E and 99°E. American lightning center is at 90°W in June, July and August and 63°W in other months. The size of each source region is assumed to be 3000 km $\times$ 3000 km with the lightning discharges uniformly distributed in this region. Having assumed that the power of lightning activity in southeast Asia, Africa, and South America follows Gaussian distributions with universal time t, lightning power variations in these three regions can be represented as $P_i = A_i e^{\left(\frac{t-T_i}{w_i}\right)^2} + c_i$ (i = 1, 2, 3), respectively, where A_i, T_i, and w_i indicate the magnitude, central time, and time width of the lightning activity, and c_i is the background level of the lightning activity in each region.

[9] The global lightning activity is inversely derived by a continuous Genetic Algorithm (GA) optimization method [*Haupt and Haupt*, 2004, p. 51]. The integration of the square of the difference between our FDTD results and the experimental measurements reported by *Price and Melnikov* [2004] is chosen as the cost function in the optimization.

[10] Thirteen parameters (three sets of A_i, T_i, w_i, and c_i, as well as a DC component corresponding to the background produced by the lightning discharges outside those three lightning centers) constitute the input vector of the GA simulations. This input vector is also called chromosome in GA method. All of those parameters in the chromosomes are adjusted to minimize the cost function. A population of 80 chromosomes are randomly generated to start the GA. In every iteration, we run GA 80 times with each input vector

(chromosome) to get their respective cost values. 20 most-fit chromosomes with smaller cost function values are preserved to reproduce 60 new vectors (offspring) in the next generation to repeat next iteration. This procedure is called "Mating." Heuristic crossover [*Haupt and Haupt*, 2004, p. 58] is employed in the chromosome mating process. We choose a mutation of 20% indicating that $0.2 \times 13 \times 80 \simeq 208$ variables are randomly mutated in each generation [*Haupt and Haupt*, 2004, p. 60]. All the details of the GA operations are given by *Haupt and Haupt* [2004, and references therein].

[11] Three modeling receivers are located at the locations corresponding to the SR field stations at Nagycenk (NCK: 47.6°N, 16.7°E, Hungary) [*Sátori and Zieger*, 1996], Mitzpe Ramon (MR: 35.45°E, 30.35°N, Israel) [*Price and Melnikov*, 2004], and Hornsund (HRN: 77°N, 15.5°E) [*Neska and Sátori*, 2006]. The vertical electrical field component (E_r) and magnetic component in north-south (H_{NS}) direction are calculated and compared with experimental measurements reported by *Sátori and Zieger* [1996] and *Price and Melnikov* [2004]. The SR eigenfrequencies of the cavity are evaluated using the Prony's method by fitting the time domain E_r data (the total sampling time is 1.6 s) with complex polynomials [*Hildebrand*, 1956, p. 379; *Füllekrug*, 1995]. The total sampling time is equivalently defined as the FDTD step time (Δt) multiplied by the total number of time domain data points. A distinction needs to be made between modal frequencies and measured peak frequencies (frequency at which the peak amplitude is measured). Modal frequencies depend on the ionospheric properties and the geometric structure of the Earth-ionosphere cavity that are independent of sources and observers, whereas measured peak frequencies depend on the source-observer relationship. The frequencies derived by the Prony's method in this paper are the modal frequencies of the cavity (see further discussion in our previous papers [*Yang and Pasko*, 2005, and references cited therein]).

3. Results

[12] Figure 1 shows north-south migrations of lightning activity in America, Africa, and Asia [*Sátori et al.*, 2003]. It is clearly observed that lightning activity occurs mainly in the summer hemisphere, moving from one hemisphere to the other during the annual cycle. From April to October, the lightning centers in these three regions are all located in Northern Hemisphere, and reach the northernmost positions during July. From October to next April, these centers move to Southern Hemisphere, and go to the southernmost locations around January. In FDTD calculations, three seasons (May, October, and January) have been simulated, and the latitudes of three lightning centers associated with each season are taken from Figure 1.

[13] The dashed lines shown in Figures 2a and 2c are experimental H_{NS} measurements of the first SR mode as a function of universal time detected at MR [*Price and Melnikov*, 2004] and HRN station in May. Those measured H_{NS} data are applied as the aim function in GA optimization. The fitting curves (solid lines in Figures 2a and 2c) are calculated by our FDTD model with the optimized lightning activity in May. The magnitude (A_i), width (w_i), central time (T_i), and background level (c_i) in three centers are adjusted by GA, leading to a good fitting presented in Figures 2a and 2c. All of those parameters are also shown in Tables 1 and 2. The associated optimized diurnal variation patterns of the lightning activity in Asia, Africa, and America derived from H_{NS} data detected at MR and HRN stations are given in Figures 2b and 2d, respectively. Two peaks appear at 0800 and 1200 UT corresponding to the maximum lightning activity in Asia and Africa, respectively. American lightning peak appears at 1900 UT in the MR data, but at 2300 UT in the HRN data. Africa has the strongest lightning activity. American lightning is weaker than that in other two regions. In October, as shown in Figures 3b and 3d, African lightning is still stronger than other two regions. American lightning intensity becomes stronger, and ranks second in these three regions. From the results derived from MR data in January (see Figure 4b), Asian lightning activity reaches its maximum in the annual cycle, about 2 times greater than that in May and October, and becomes the dominant one in the cavity. During the same time period, African lightning activity goes to its minima. However, the results derived from the observations at HRN station (see Figure 4d) give a different pattern, in which African lightning is still the strongest one, and Asian lightning is weakest. Diurnal frequency variation of the first SR mode (Figures 5 and 6) is derived from E_r component received at the simulated NCK station in the FDTD calculations using the diurnal variation pattern of the lightning activity shown in Figures 2–4.

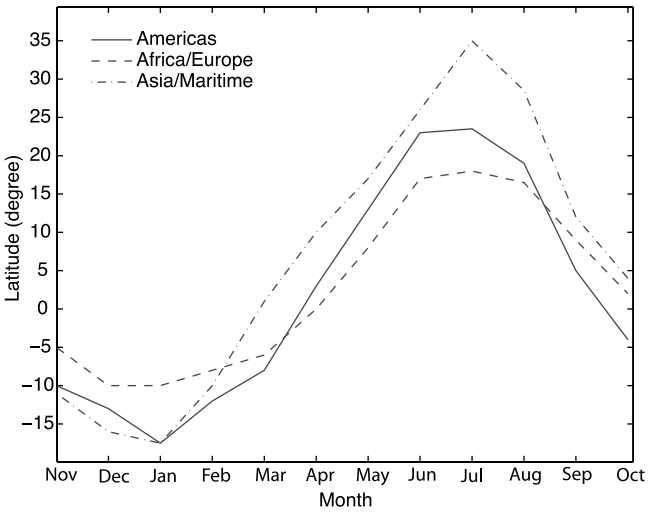

Figure 1. Seasonal north-south variations of the centers of the meridional lightning distributions corresponding roughly to the Americas, Africa/Europe, and the Asia/Maritime continent [*Sátori et al.*, 2003].

4. Discussion

[14] In H_{NS} power of the first SR mode shown in Figures 2–4, two peaks at approximately 0800 and 2000 UT corresponding to maximum of lightning activity in Asia and America are clearly observed. Since the Africa is placed in the node of the antenna pattern, the evaluation of Africa should provide a larger error than that of the other two centers. H_{EW} component is a better candidate to calculate African lightning. However, owing to the geometry of the

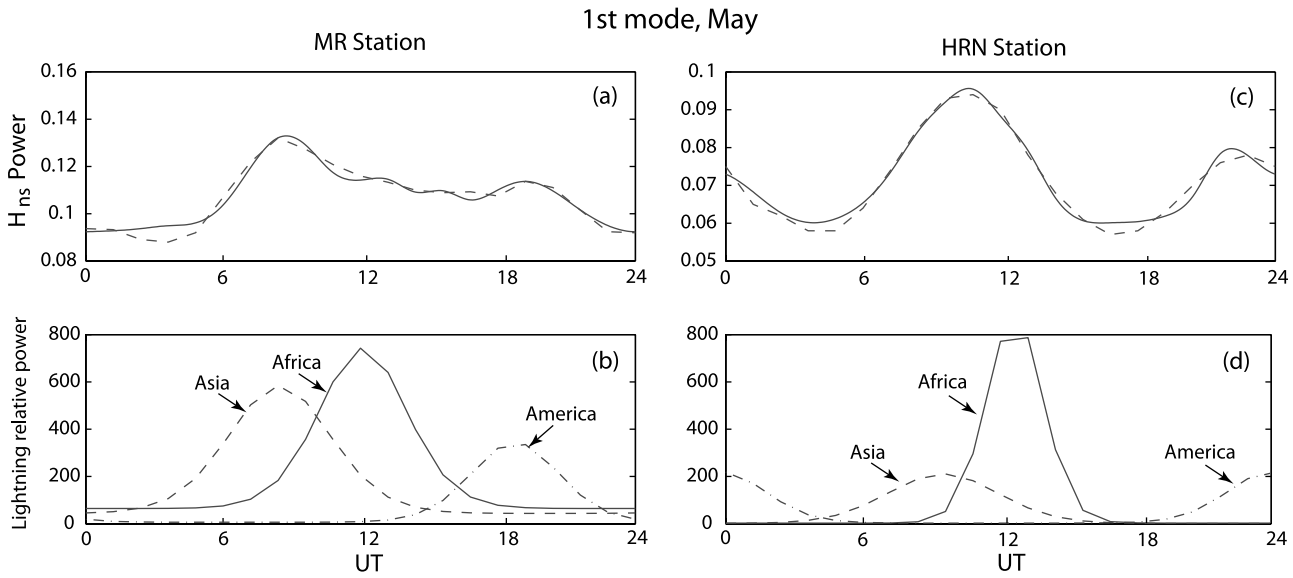

Figure 2. Comparison of diurnal H_{NS} power variations of the first SR mode in May measured at (a) MR [*Price and Melnikov*, 2004] and (c) HRN stations (dashed line) with the results derived using FDTD method (solid line). The distributions of the lightning activity in Asia, Africa, and America derived in May by GA optimization obtained using (b) MR and (d) HRN data.

source and receiver, America and Asia are placed at the nodes of receiver antenna for H_{EW} component. In the work by *Price and Melnikov* [2004], we can find that the experimental H_{EW} measurement only has one peak corresponding African lightning activity. We tried H_{EW} component, but the error of the derived American and Asian lightning activity is too high to be acceptable. That is why we only use the H_{NS} component. However, we note that both H_{NS} or H_{EW} components cannot accurately reproduce the lightning activity in all three lightning regions individually. Therefore, in the future SR measurements, an optimal angle should be determined for the antenna installation on the basis of the geometry of the source and receiver in each season, which would allow to accurately extract the lightning activity information in three regions using one magnetic field component.

[15] In the simulations, the H_{NS} power spectrum is chosen as the aim function in GA optimization. Since GA optimization method randomly selects the results to minimize the cost function during iterations, its results are not exactly the same in every simulation. A set of GA simulations have been conducted. The results vary in the range of 5% and have the same features which are illustrated in Figures 2–4 (e.g., the ranking of the lightning magnitude at three centers).

[16] In Figures 2–4, lighting activity in Asia, Africa, and America reaches maximum at approximately 0800, 1200 and 2000 UT, respectively. Obvious seasonal power variations of the lightning activity in Asia, Africa and America are observed in Figures 2–4. The results derived from MR data indicate that African lightning has the strongest power level of the three centers in May, and American lightning goes to the weakest level at the same time (see Figure 2b). In October, lighting activity in Asia and Africa are both reduced to 70% of their level in May. Americas become the second strongest of the three regions. The consistent features can be also clearly found in Figures 2d and 3d, which are obtained using the measurements at HRN station. The cause of African maximum lightning activity in May, comparing to its own level in October and January is attributable to the widening African land mass occupied by lightning activity when lightning migrates northward in May and switching on also the European thunderstorms (see Figures 2b and 2d). Since the Amazon basin is still in "Green Ocean" regime in May following the wet season with heavy rainfall but with infrequent lightning, Asia has higher lightning activity than in Americas in this month (see Figure 2b) in accordance with OTD satellite observations [*Christian et al.*, 2003]. In October and November, South American lightning activity reaches its highest level in the

Table 1. Relative Magnitude Maximum, Center Time, and Width of the Lightning Activity at Africa, Asia, and America Derived From SR Measurements at MR Station[a]

Lightning	May			October			January		
Centers	A_m	t_c	t_w	A_m	t_c	t_w	A_m	t_c	t_w
Africa	777.5	12.3	2.32	556.4	11.87	2.19	498.4	12.1	2.36
Asia	584.5	8.52	2.97	363.8	8.92	3.23	339.9	8.33	3.09
America	309.1	18.71	2.49	439.0	19.12	3.21	348.5	19.3	3.87

[a]Relative magnitude maximum, A_m; center time, t_c; and width, t_w.

Table 2. Relative Magnitude Maximum, Center Time, and Width of the Lightning Activity at Africa, Asia, and America Derived From SR Measurements at HRN Station[a]

Lightning	May			October			January		
Centers	A_m	t_c	t_w	A_m	t_c	t_w	A_m	t_c	t_w
Africa	795.2	12.6	1.62	625.5	12.5	1.92	561.2	12.2	1.72
Asia	207.4	9.34	3.14	144.2	9.8	3.54	221.3	8.1	3.04
America	201.3	23.9	2.84	284.7	19.8	3.33	274.5	19.9	3.94

[a]Relative magnitude maximum, A_m; center time, t_c; and width, t_w.

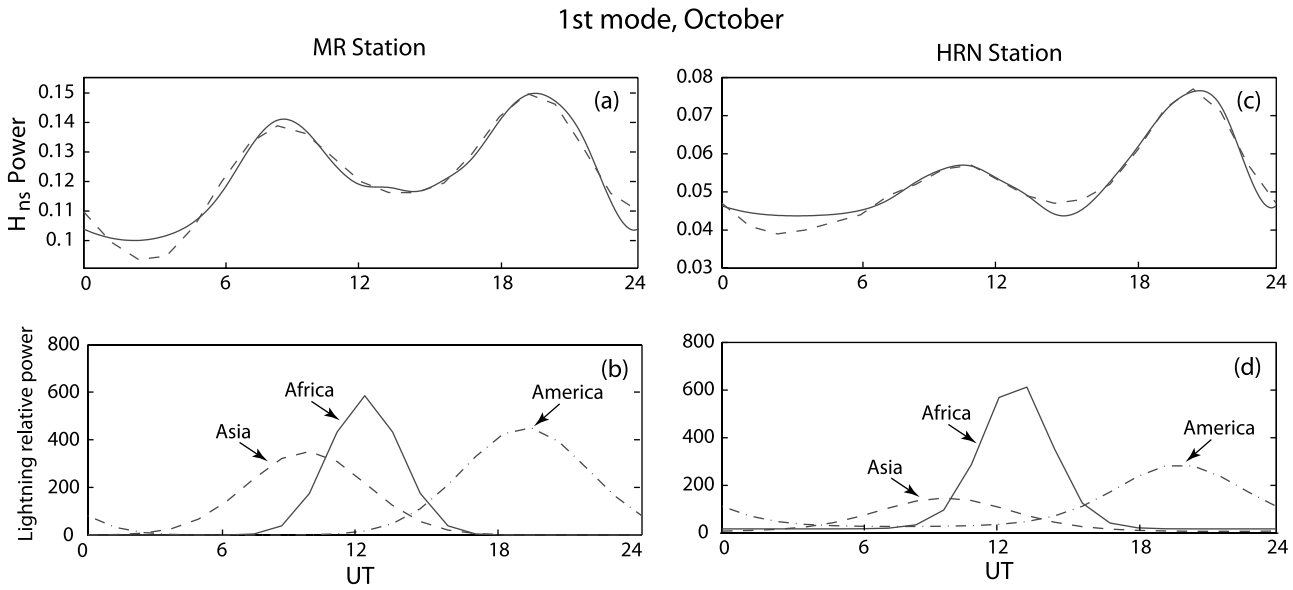

Figure 3. Comparison of diurnal H_{NS} power variations of the first SR mode in October measured at (a) MR [*Price and Melnikov*, 2004] and (c) HRN stations (dashed line) with the results derived using FDTD method (solid line). The distributions of the lightning activity in Asia, Africa, and America derived in October by GA optimization obtained using (b) MR and (d) HRN data.

annual cycle owing to the thermodynamical and hydrological conditions favorable there for lightning generation [*Williams and Sátori*, 2004].

[17] Consistent with measurements reported by *Sentman and Fraser* [1991], African lightning activity becomes the strongest among the three regions in April and increases by 50% in comparison with its September level. Conversely, in September, the magnitude of American lighting becomes greater than that of the other two regions, and approximately 25% greater than that in April. Although the data from *Sentman and Fraser* [1991] were collected in April and September, 1 month earlier than the months we studied in our simulations, all of these features can be still found in the solution of the inverse problem. However, in contrast with our results, Asian lightning activity in both April and September has the same magnitude in the work by *Sentman and Fraser* [1991], and always is the weakest one among the three lightning regions during both months.

[18] In January, African lighting is reduced to its minimum in the annual cycle. American lightning keeps the

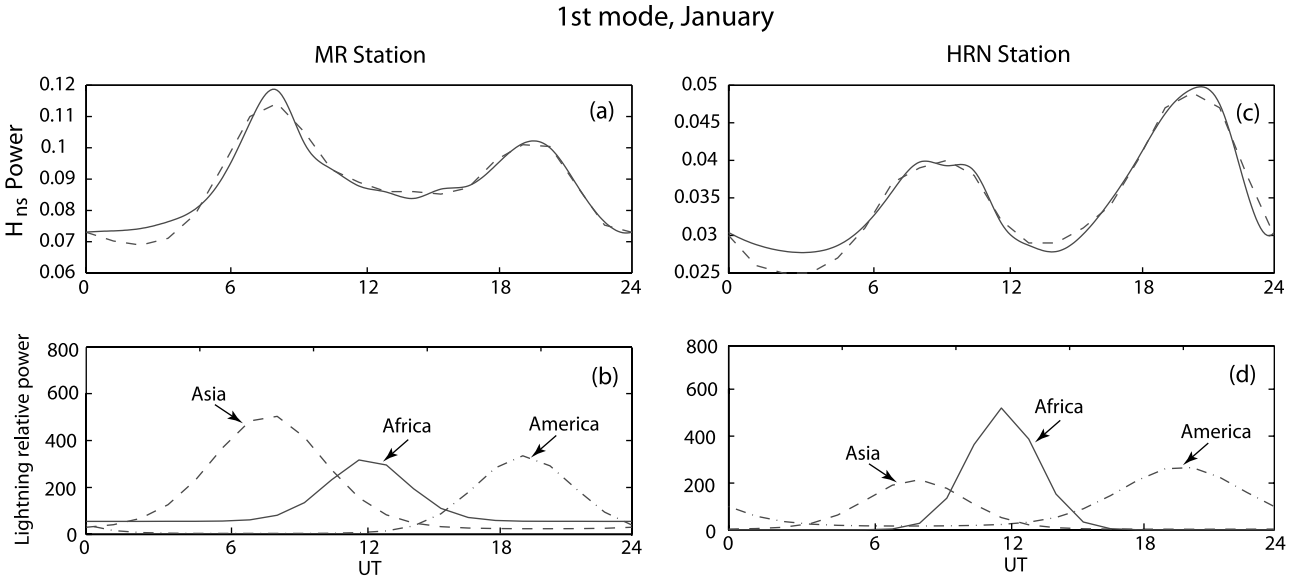

Figure 4. Comparison of diurnal H_{NS} power variations of the first SR mode in January measured at (a) MR [*Price and Melnikov*, 2004] and (c) HRN stations (dashed line) with the results derived using FDTD method (solid line). The distributions of the lightning activity in Asia, Africa, and America derived in January by GA optimization obtained using (b) MR and (d) HRN data.

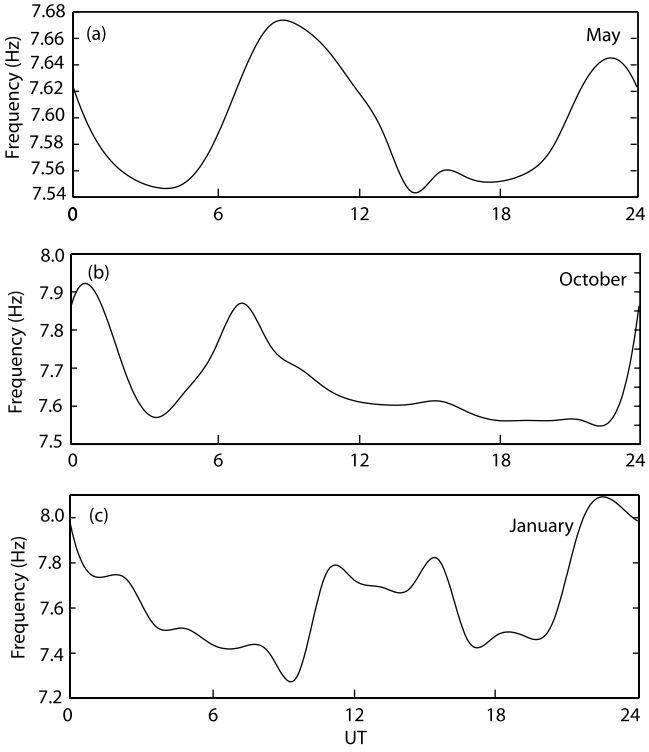

Figure 5. Diurnal frequency variation of the first SR mode at NCK station in (a) May, (b) October, and (c) January with the lightning distributions derived from the measured data at MR station.

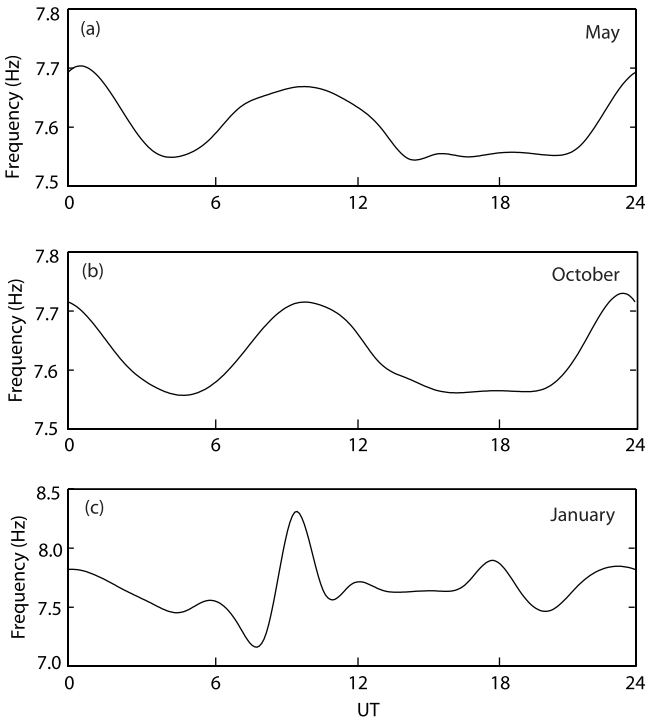

Figure 6. Diurnal frequency variation of the first SR mode at NCK station in (a) May, (b) October, and (c) January with the lightning distributions derived from the measured data at HRN station.

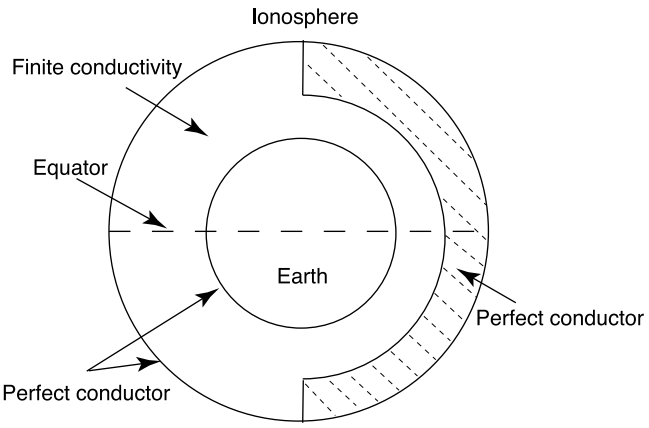

Figure 7. Cavity with artificially asymmetric conductivity. The height of half cavity is 100 km. For another half, the height is 50 km.

same level as that in October. The maximum of Asian lightning appears during this season, and is approximately 2 times as great as in the other two regions (see Figure 4b). However, in Figure 4d, African lightning activity derived from HRN data is still the strongest one in three regions. The discrepancy between MR and HRN with relation to Asian and American activity in January (Figure 4) might be attributed to the day-night asymmetry problem. HRN station is completely under local night condition in January. Both Asian and American lightning activities are detected under same local condition, so HRN station indicates the proper ranking for America and Asia in January. In the case of MR, Asian lightning is observed under local daytime condition while American lightning activity is measured when MR is under local nighttime condition. Therefore, the power peak associated with American lightning activity detected at MR is weaker than Asian peak, while American peak is stronger at HRN station in January.

[19] Since the simulated receiver is covered by the lightning source region centered at the latitude shown in Figure 1 in July, the detected SR signals are mixed with the strong near field close to the simulated lightning sources. SR power spectrum cannot be accurately derived for this month. Therefore, we do not report the simulation results in July.

[20] Some related results detected by the Optical Transient Detector (OTD) have been given by *Christian et al.* [2003]. These space-borne records might be used as a starting point for further analysis. The diurnal variation of the source activity was modeled [*Hayakawa et al.*, 2005; *Nickolaenko et al.*, 2006], and the SR patterns were obtained on the basis of the OTD data [*Greenberg and Price*, 2007]. The latter publication indicates the prevalence of Asian activity. In OTD data, Africa is the most active lightning center with the highest annualized flash rate, and Americas rank second. Flash density is generally greatest during the respective hemisphere's spring and summer seasons over land and year round in coastal zones. In Figure 6b of *Christian et al.* [2003], lightning activity in Africa is the most intensive in May, and America has much weaker lightning activity than other two regions, which agrees with our result shown in Figure 2b. Furthermore,

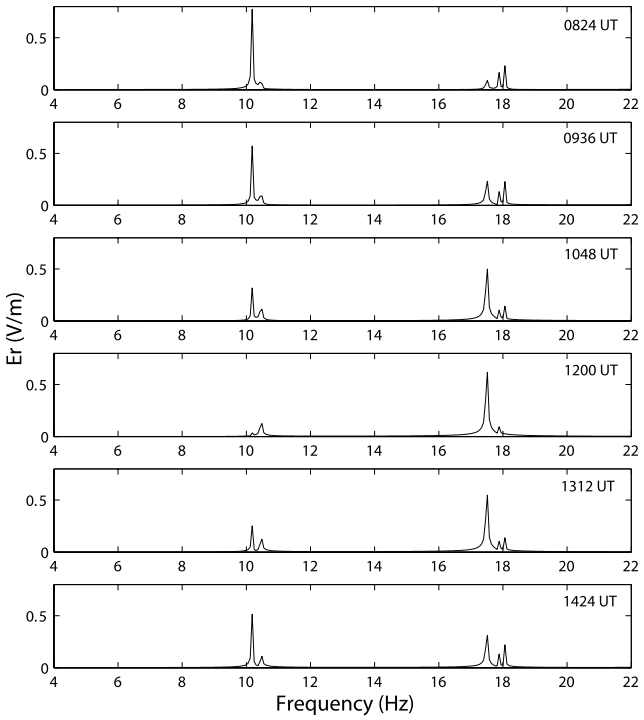

Figure 8. FDTD results derived from an artificially asymmetric cavity shown in Figure 7 assuming free space inside the cavity. A single source (3000 km by 3000 km) moves around the Earth on the equator synchronized with the motion of the day-night terminator, and is activated in regions corresponding to local afternoon in the cavity.

OTD data reveal that Africa has stronger lighting activity than America, and Asia is the region having the weakest lightning activity among the three lightning centers in October. The same features can be also observed in Figures 3b and 3d. In January, the result derived from HRN measurements is consistent with OTD data (see Figure 4d). However, a disagreement appears between our FDTD results and OTD measurement in Figure 4b. Asian lightning region becomes much stronger than the other two regions in our FDTD simulations, while Africa still has the highest lightning flash rate shown in Figure 6a of *Christian et al.* [2003]. However, the work reported by *Hayakawa* [1989] dealing with satellite radio (ELF/VLF) observation by Ariel 4 Satellite at 3.2 kHz indicates the Asian predominance. Since OTD data includes both intracloud and cloud-to-ground lightning discharges, and Schumann resonances are mainly produced by the cloud-to-ground lightning, it might be an explanation for this disagreement. A similar problem has been discussed by *Greenberg and Price* [2007].

[21] Another important explanation for this difference is the geometry of the locations of the lightning centers and the observing station. In spring and fall seasons, African lighting center is close to MR station in Israel [*Price and Melnikov*, 2004], and source-observer orientation angle (angle between the plane of the source-observer great circle path and the plane of the north-south meridional circle of the observer) is relatively big. African lighting activity can produce magnetic field in north-south direction at MR station with a reasonable level for the inverse calculation using our optimization method. However, the central time of African lightning shown in Figures 2b and 3b (1200–1300 UT) is about 2 hours earlier than those reported by, for example, *Sentman and Fraser* [1991] (1400–1600 UT). In January, African lightning activity moves southward leading to the decrease of the source-observer orientation angle. African lighting activity makes a smaller contribution to the H_{NS} component. Therefore, the quality of the experimental data directly influence the precision of the inverse calculation. Small deviation in the experimental SR H_{NS} data can lead to a significant inaccuracy in African lighting intensity inversely derived by our optimization method. Besides Africa, the lighting activity in other two centers is also effected by the quality of the measured data. In Figure 2b, American lightning reaches peak around 2000 UT, while the central time of American lighting activity is approximately 2300 UT shown in Figure 2d. Both North America (NA) and South America (SA) are active in May. HRN is rather close to NA on the great circle path. NA has its peak activity at 2200–2300 UT, while SA local afternoon at 1900–2000 UT. MR station (H_{NS}) is more responsive to the SA lightning activity while HRN (H_{NS}) is sensitive to NA.This is the reason why the H_{NS} field component at MR and HRN indicate maximum lightning activity for Americas at different UT time points.

[22] The diurnal frequency variations of the first SR mode (E_r component) for NCK station with GA optimized lightning activity are shown in Figures 5 and 6. The magnitude of the lightning activity in three centers are taken from Figures 2–4. In May, the frequency goes to the maximum (7.67 Hz) around 1000 UT, and reaches the minimum (7.55 Hz) approximately 1900 UT. The total magnitude of the variation is approximately 0.12 Hz. In the measurements reported by *Sátori and Zieger* [1996], *Sátori et al.* [1996], and *Ondrášková et al.* [2007], the magnitude of the frequency variation is also approximately 0.1 Hz. In October, the frequency maximum appears at 0800 UT, and still has similar variation tendency with that in May (see Figures 5b and 6b). In January, the situation is significantly different. SR frequency decreases during initial several hours in the diurnal cycle, and a sharp jump of frequency appears around 1000 UT in both Figures 5c and 6c.

[23] The frequency variations were reported by *Sátori and Zieger* [1996] and [*Sátori et al.* [1996] in connection with ENSO since 1996. Relevant modeling was made with the three sources shifted southward [see *Nickolaenko and Hayakawa*, 2002, Figure 6.22]. Similar features have been reported between our FDTD results and their experimental winter measurements. We believe that the different frequency variations during different seasons can be explained by the seasonal variations of lighting activity. In spring and summer (May to September), African lightning center is located in Northern Hemisphere with the latitude exceeding 10°. Its distance to NCK station is less than 4000 km. The other two centers are approximately at the distances of 10,000 km from the station close to nulls of spatial field distribution of the first SR mode E_r component. Furthermore, African lightning activity reaches its maximum, and is much stronger than at other two centers during summertime. An additional FDTD simulation, in which only one source is located at Africa, has been performed. The result is in a good agreement with that shown in Figure 5a with a maximum at around

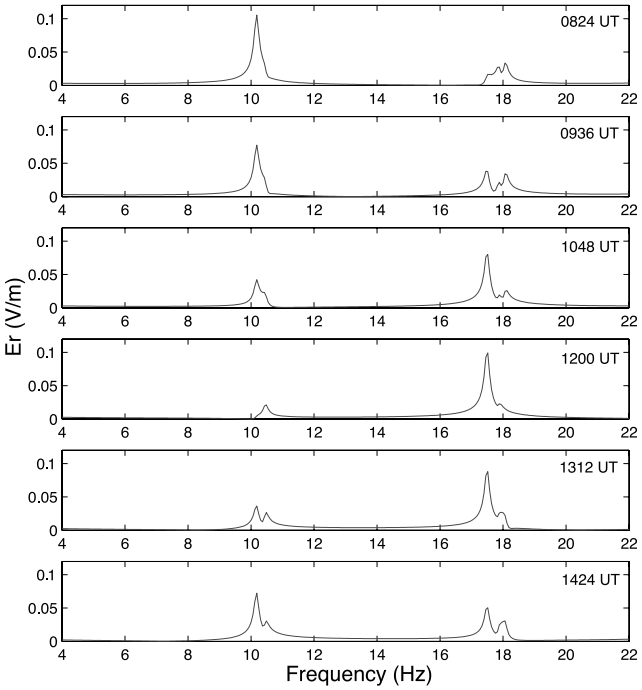

Figure 9. Same as Figure 8 but assuming a uniform conductivity 8×10^{-12} S/m inside the cavity.

1000 UT. Therefore, we believe that the magnitude of E_r component and its frequency variation detected at NCK station are mainly determined by the waves from Africa in spring and summer.

[24] In October, African lightning moves southward to equator, and its influence at NCK station decreases owing to the spatial distribution of E_r component [*Yang and Pasko*, 2007]. Although the lightning activity in Asia and America shows more influence on the frequency variation, African lightning activity is still the most significant one to control the frequency variation. Therefore, the results shown in Figures 5b and 6b are similar to those shown in Figures 5a and 6a. In January, African lighting center moves to its southernmost position in the annual cycle (7000 km to NCK station), and its magnitude is reduced to the level about half value of that in summer. Therefore, the lightning activity in other two regions becomes the dominant one to control SR frequency in winter.

[25] To provide additional insight on SR frequency variations, a set of additional FDTD simulations has been performed. In these simulations, an artificially asymmetric cavity as shown in Figure 7 is employed. Half cavity has a height of 100 km, and another half has height of 50 km. The half cavity with a height of 50 km accounts for the Earth-ionosphere cavity at daytime, and the other half accounts for the cavity at night. A single source (3000 km by 3000 km) moves around the Earth on the equator synchronized with the motion of the day-night terminator, and is always activated in regions at local afternoon in the cavity.

[26] Figure 8 shows FDTD results derived from the cavity (shown in Figure 7) without the inclusion of the conductivity between the perfectly conducting boundaries forming the cavity. Owing to the asymmetry of the cavity, the first SR mode is split into two frequencies. One is 10.1 Hz (f_1), and another is 10.45 Hz (f_2). Here, we define the modes with the frequencies f_1 and f_2 as modes M_1 and M_2, respectively. The modes M1 and M2 correspond to eigenfunctions $P_1(\cos(\theta)) = \cos(\theta)$ and $P_1^1(\cos(\theta))\exp(\pm i\phi) = \sin(\theta)\exp(\pm i\phi)$. The latter are double degenerate, i.e., have the coincident eigenvalues. Note, that θ denotes now the angular distance from the center of the day hemisphere to an arbitrary point rather than the source [*Nickolaenko and Hayakawa*, 2002]. At 0824 and 0936 UT, the magnitude of M_1 is much stronger than that of M_2. At 1048 UT, the receiver is close to the nodal line of the first SR mode. The magnitude of M_1 and M_2 decreases and increases, respectively. At 1200 UT, the receiver passes the nodal line. The M_2 magnitude becomes much stronger than that of M_1. Since the receiver is close to the nodal line of the first SR mode at 1048 and 1200 UT, the magnitude of first SR mode is much weaker at these times than at other times. After 1200 UT, the magnitude of M_1 increases, and the M_2 magnitude decreases to the level at 0824 UT. For test purposes, several different conductivity profiles are employed in Figures 9, 10, and 11 to observe the variation of the mode splitting spectrum due to variation of conductivity within a cavity from zero to the experimental values. Figure 9 shows the spectrum derived with a conductivity equal to 8×10^{-12} S/m. The spectrum of the resonance modes becomes wider and flatter owing to the conducting losses in the cavity. The modes with weak magnitudes (e.g., peaks at 10.45 Hz at 0824 and 0936 UT) are merged into the adjacent strong modes. However, two splitting frequencies can be still observed in the plots corresponding to 1312 and 1424 UT. With the conductivity increasing to 3×10^{-11} S/m (shown in Figure 10), all splitting modes of the first SR mode are merged together and form one single peak. A jump of the first peak frequency is clearly observed between

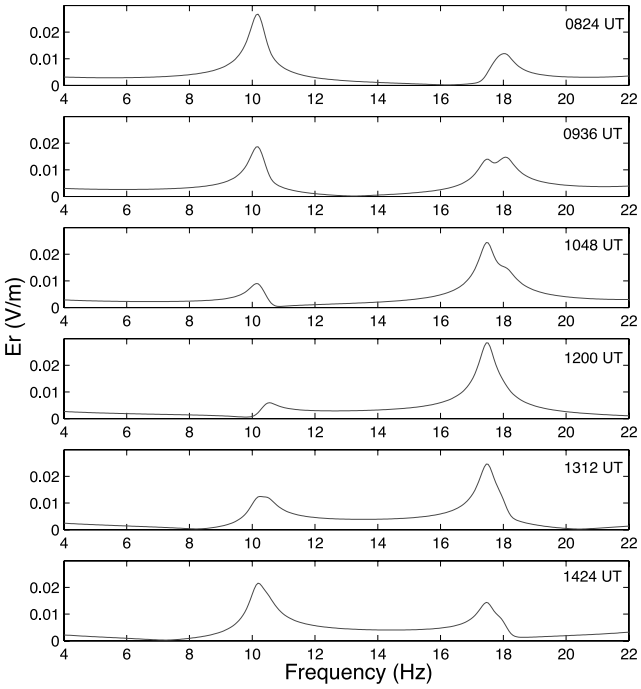

Figure 10. Same as Figure 8 but assuming a uniform conductivity 3×10^{-11} S/m inside the cavity.

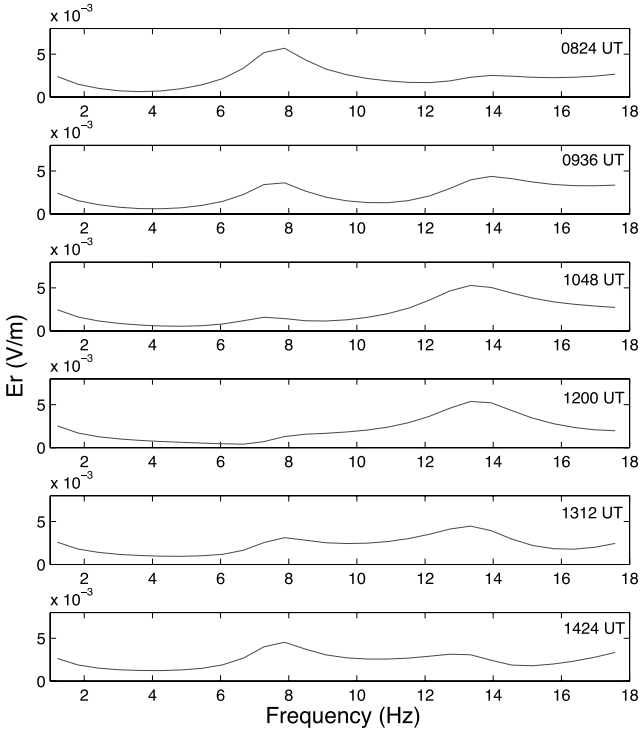

Figure 11. Same as Figure 8 but assuming a conductivity derived from International Reference Ionosphere model inside the cavity.

1048 and 1200 UT. Figure 11 shows FDTD results derived for a cavity with a realistic conductivity calculated from the IRI model. A jump of the first peak frequency is also clearly observed between 1048 and 1200 UT. We believe that this frequency jump comes from the mode splitting, which is clearly observed in Figure 8 (1048 UT and 1200 UT). As shown in Figure 8, when the receiver is close to the nodal line, M_1 is much stronger than M_2 at 1048 UT. When the receiver passes the nodal line, the magnitude of M_1 quickly decreases, and M_2 becomes much stronger than M_1. This behavior is similar to modeling results presented by *Sentman* [1996], where frequency variations occur as a result of nodal effects.

[27] Since one of the splitting modes is much weaker than another one, Prony's method, which we used to find the eigenfrequency of the cavity, can only detect the strongest splitting mode. Furthermore, we also note that the peak frequency, which was employed in previous studies [e.g., *Sátori and Zieger*, 1996; *Ondrášková et al.*, 2007] also follows the strongest splitting mode. Therefore, the singularity-like frequency jump appearing at around 1000 UT in Figures 5c and 6c could be produced by Asian lightning maximizing from 0500 to 1000 UT when the receiver passes the nodal line. All of the features of the different frequency variations in different seasons, which are shown in Figures 5c and 6c can also be found in the measurements reported by *Ondrášková et al.* [2007]. In Figure 3 of *Ondrášková et al.* [2007], a frequency peak appears at 1000 UT, for the time period from June to September when African lightning activity reaches maximum. From November to March when African lightning becomes weaker and move southward, the frequency decreases during 0000 to 1000 UT time period, then reaches the maximum value around 1500 UT.

5. Conclusions

[28] 1. A GA optimization method has been employed to inversely calculate the intensity of lightning activity in Asia, Africa, and America using the measured H_{NS} component of the first SR mode from two different SR stations, and consistent results on the diurnal variations of the lightning activity in Africa, Asia, and America are clearly observed employing the measured data at these two stations.

[29] 2. The simulated lightning distributions in three regions are in a good agreement with OTD measurements in May and October. From the results derived by GA method at MR station, Asia has the most intensive cloud-to-ground lightning activity in January, which is in agreement with other SR modeling [*Greenberg and Price*, 2007]. We believe that the precision of this GA method is directly influenced by the quality of the experimental SR data, especially when African lightning center moves to the southernmost position in January. Small deviation in the experimental SR H_{NS} data can lead to a significant inaccuracy in African lighting intensity inversely derived by our optimization method in winter. Since both H_{NS} or H_{EW} components cannot accurately reproduce the lightning activity in all three lightning regions individually, we suggest that an optimal angle of the antenna installation need to be determined on the basis of the geometry of the source and receiver in the future experimental measurements in each season, which would allow to accurately extract the lightning activity in three regions using only one magnetic field component in this optimized direction.

[30] 3. The SR frequency variation depends on the positions and variations of the lightning activity in the three lightning centers. Owing to their positions with respect to the observing station and their seasonal variations, the three lightning centers make different contributions to the frequency variations. Modeling results indicate that the difference between the frequency variation experimentally detected during summer and winter is caused by the mode splitting effects associated with the fact that the lightning activity in Africa and Asia become the dominant one in Earth-ionosphere cavity during summer and winter, respectively.

[31] **Acknowledgments.** The authors thank Mariusz Neska for making available SR data from Hornsund, at Polish Polar Station. The contribution of Heng Yang and Victor Pasko was supported by NSF ATM-0734083 grant to Penn State University. Gabriella Sátori's contribution was supported by Hungarian Science Foundation (grant K72474). We thank three reviewers for many useful comments.

References

Ando, Y., and M. Hayakawa (2007), Use of generalized cross validation for identification of global lightning distribution by using Schumann resonances, *Radio Sci.*, *42*, RS2S16, doi:10.1029/2006RS003481.

Ando, Y., M. Hayakawa, A. V. Shvets, and A. P. Nickolaenko (2005), Finite difference analyses of Schumann resonance and reconstruction of lightning distribution, *Radio Sci.*, *40*, RS2002, doi:10.1029/2004RS003153.

Berenger, J. P. (2002), FDTD computation of VLF-LF propagation in the Earth-ionosphere waveguide, *Ann. Telecommun.*, *57*(11–12), 1059.

Bilitza, D. (2001), International Reference Ionosphere 2000, *Radio Sci.*, *36*(2), 261.

Christian, H. J., et al. (2003), Global frequency and distribution of lightning as observed from space by the Optical Transient Detector, *J. Geophys. Res.*, *108*(D1), 4005, doi:10.1029/2002JD002347.

Cummer, S. A. (2000), Modeling electromagnetic propagation in the Earth-ionosphere waveguide, *IEEE Trans. Antennas Propag.*, *48*(9), 1420.

Füllekrug, M. (1995), Schumann-resonances in magnetic-field components, *J. Atmos. Terr. Phys.*, *57*(5), 479.

Greenberg, E., and C. Price (2007), Diurnal variations of ELF transients and background noise in the Schumann resonance band, *Radio Sci.*, *42*, RS2S08, doi:10.1029/2006RS003477.

Greifinger, P., V. Mushtak, and E. Williams (2005), The lower characteristic ELF altitude of the Earth-ionosphere waveguide: Schumann resonance observations and aeronomical estimates, in *VI International Symposium on Electromagnetic Compatibility and Electromagnetic Ecology: The Proceedings*, pp. 250–254, Inst. of Electr. and Electron. Eng., New York.

Greifinger, P. S., V. C. Mushtak, and E. R. Williams (2007), On modeling the lower characteristic ELF altitude from aeronomical data, *Radio Sci.*, *42*, RS2S12, doi:10.1029/2006RS003500.

Hale, L. C. (1984), Middle atmosphere electrical structure, dynamics, and coupling, *Adv. Space Res.*, *4*, 175.

Haupt, R. L., and S. E. Haupt (2004), *Practical Genetic Algorithms*, John Wiley, Hoboken, N. J.

Hayakawa, M. (1989), Satellite observation of low-latitude VLF radio noises and their association with thunderstorms, *J. Geomagn. Geoelectr.*, *41*, 573.

Hayakawa, M., and T. Otsuyama (2002), FDTD analysis of ELF wave propagation in inhomogencous subionospheric waveguide models, *Appl. Comput. Electromagn. Soc. J.*, *17*, 239.

Hayakawa, M., M. Sekiguchi, and A. P. Nickolaenko (2005), Diurnal variations of electric activity of global thunderstorms deduced from OTD data, *J. Atmos. Electr.*, *25*, 55.

Hildebrand, F. B. (1956), *Introduction to Numerical Analysis*, McGraw-Hill, New York.

Hu, W., and S. A. Cummer (2006), An FDTD model for low and high altitude lightning-generated EM fields, *IEEE Trans. Antennas Propag.*, *54*(5), 1513.

Huang, E., E. Williams, R. Boldi, S. Heckman, W. Lyons, M. Taylor, T. Nelson, and C. Wong (1999), Criteria for sprites and elves based on Schumann resonance observation, *J. Geophys. Res.*, *104*(D14), 16,943.

Kirillov, V. V. (2002), Solving a two-dimensional telegraph equation with anisotropic parameters, *Radiophys. Quantum Electron.*, *45*, 929.

Kirillov, V. V. (2005), Two-dimensional theory of elf electromagnetic wave propagation in the earth-ionosphere waveguide channel, *Radiophys. Quantum Electron.*, *48*, 737.

Morente, J. A., G. J. Molina-Cuberos, J. A. Port, B. P. Besser, A. Salinas, K. Schwingenschuch, and H. Lichtenegger (2003), A numerical simulation of Earth's electromagnetic cavity with the Transmission Line Matrix method: Schumann resonances, *J. Geophys. Res.*, *108*(A5), 1195, doi:10.1029/2002JA009779.

Mushtak, V. C., and E. Williams (2002), ELF propagation parameters for uniform models of the Earth-ionosphere waveguide, *J. Atmos. Solar Terr. Phys.*, *64*(18), 1989.

Neska, M., and G. Sátori (2006), Schumann resonance observation at Polish Polar Station at Spitsbergen as well as in Central Geophysical Observatory in Belsk, Poland, *Przegl. Geofiz.*, Engl. Transl., no. 3–4, 189.

Nickolaenko, A. P., and M. Hayakawa (2002), *Resonances in the Earth-Ionosphere Cavity*, Kluwer Acad., Norwell, Mass.

Nickolaenko, A. P., G. Sátori, V. Ziegler, L. M. Rabinowicz, and I. G. Kudintseva (1998), Parameters of global thunderstorm activity deduced from the long-term Schumann resonance records, *J. Atmos. Solar Terr. Phys.*, *60*, 387.

Nickolaenko, A. P., M. Hayakawa, and M. Sekiguchi (2006), Variations in global thunderstorm activity inferred from the OTD records, *Geophys. Res. Lett.*, *33*, L06823, doi:10.1029/2005GL024884.

Ondrášková, A., P. Kostecký, S. Ševčík, and L. Rosenberg (2007), Long-term observations of Schumann resonances at Modra Observatory, *Radio Sci.*, *42*, RS2S09, doi:10.1029/2006RS003478.

Otsuyama, T., D. Sakuma, and M. Hayakawa (2003), FDTD analysis of ELF wave propagation and Schumann resonances for a subionospheric waveguide model, *Radio Sci.*, *38*(6), 1103, doi:10.1029/2002RS002752.

Pasko, V. P., U. S. Inan, T. F. Bell, and Y. N. Taranenko (1997), Sprites produced by quasi-electrostatic heating and ionization in the lower ionosphere, *J. Geophys. Res.*, *102*(A3), 4529.

Pasko, V. P., U. S. Inan, T. F. Bell, and S. C. Reising (1998), Mechanism of ELF radiation from sprites, *Geophys. Res. Lett.*, *25*(18), 3493.

Price, C., and A. Melnikov (2004), Diurnal, seasonal and inter-annual variations of the Schumann resonance parameters, *J. Atmos. Solar Terr. Phys.*, *66*, 1179.

Sato, M., and H. Fukunishi (2003), Global sprite occurrence locations and rates derived from triangulation of transient Schumann resonance events, *Geophys. Res. Lett.*, *30*(16), 1859, doi:10.1029/2003GL017291.

Sátori, G., and B. Zieger (1996), Spectral characteristics of Schumann resonances observed in Central Europe, *J. Geophys. Res.*, *101*(D23), 29,663.

Sátori, G., J. Szendröi, and J. Verö (1996), Monitoring Schumann resonances—I. Methodology, *J. Atmos. Terr. Phys.*, *58*(13), 1475.

Sátori, G., E. R. Williams, and D. J. Boccippio (2003), On the dynamics of the north-south seasonal migration of global lightning, *Eos Trans. AGU*, *84*(46), Fall Meet. Suppl., Abstract AE32A-0167.

Schumann, W. O. (1952), Uber die strahlungslosen einer leitenden Kugel die von einer Luftschicht und einer Ionospharenhulle umgeben ist, *Z. Naturforsch. A*, *7*, 149.

Sekiguchi, M., Y. Hobara, and M. Hayakawa (2008), Diurnal and seasonal variations in the Schumann resonance parameters at Moshiri, Japan, *J. Atmos. Electr.*, *28*, 1.

Sentman, D. D. (1995), Schumann resonances, in *Handbook of Atmospheric Electrodynamics*, p. 267, CRC Press, London.

Sentman, D. D. (1996), Schumann resonance spectra in a two-scale-height Earth-ionosphere cavity, *J. Geophys. Res.*, *101*(D5), 9479.

Sentman, D. D., and B. J. Fraser (1991), Simultaneous observations of Schumann resonances in California and Australia: Evidence for intensity modulation by the local height of the D-region, *J. Geophys. Res.*, *96*(A9), 15,973.

Simpson, J. J. (2008), Global FDTD Maxwell's equations modeling of electromagnetic propagation from currents in the lithosphere, *IEEE Trans. Antennas Propag.*, *56*(1), 199.

Simpson, J. J., and A. Taflove (2004), Three-dimensional FDTD modeling of impulsive ELF propagation about the earth-sphere, *IEEE Trans. Antennas Propag.*, *52*(2), 443.

Simpson, J. J., and A. Taflove (2007), A review of progress in FDTD Maxwell's equations modeling of impulsive subionospheric propagation below 300 kHz, *IEEE Trans. Antennas Propag.*, *55*(6), 1582.

Soriano, A., E. A. Navarro, D. L. Paul, J. A. Porti, J. A. Morente, and I. J. Craddock (2005), Finite-difference time domain simulation of the Earth-ionosphere resonant cavity: Schumann resonances, *IEEE Trans. Antennas Propag.*, *53*(4), 1535.

Taflove, A., and S. C. Hagness (2000), *Computational Electrodynamics: The Finite-Difference Time-Domain Method*, Artech House, Boston, Mass.

Williams, E. R. (1992), The Schumann resonance—A global tropical thermometer, *Science*, *256*(5060), 1184.

Williams, E. R., and G. Sátori (2004), Lightning, thermodynamic and hydrological comparison of the two tropical continental chimneys, *J. Atmos. Solar Terr. Phys.*, *66*, 1213.

Yang, H., and V. P. Pasko (2005), Three-dimensional finite-difference time-domain modeling of the Earth-ionosphere cavity resonances, *Geophys. Res. Lett.*, *32*, L03114, doi:10.1029/2004GL021343.

Yang, H., and V. P. Pasko (2006), Three-dimensional finite-difference time-domain modeling of the diurnal and seasonal variations in Schumann resonance parameters, *Radio Sci.*, *41*, RS2S14, doi:10.1029/2005RS003402.

Yang, H., and V. P. Pasko (2007), Power variations of Schumann resonances related to El Niño and La Niña phenomena, *Geophys. Res. Lett.*, *34*, L11102, doi:10.1029/2007GL030092.

Yang, H., V. P. Pasko, and Y. Yair (2006), Three-dimensional finite-difference time-domain modeling of the Schumann resonance parameters on Titan, Venus, and Mars, *Radio Sci.*, *41*, RS2S03, doi:10.1029/2005RS003431.

Yatsevich, E. I., A. P. Nickolaenko, A. V. Shvets, and L. M. Rabinowicz (2006), Two component source model of Schumann resonance signal, *J. Atmos. Electr.*, *26*, 1.

Yee, K. S. (1966), Numerical solution of initial boundary value problem involving Maxwell's equations in isotropic media, *IEEE Trans. Antennas Propag.*, *14*(3), 802.

V. P. Pasko, CSSL Laboratory, Pennsylvania State University, 211B EE East, University Park, PA 16802, USA. (vpasko@psu.edu)

G. Sátori, Geodetic and Geophysical Research Institute, Hungarian Academy of Sciences, Csatkai u. 6-8, H-9400 Sopron, Hungary. (satori@ggki.hu)

H. Yang, Department of Electrical and Computer Engineering, University of Houston, 4800 Calhoun Road, Houston, TX 77004, USA. (hyang11@uh.edu)